
Model Alignment Search

Satchel Grant*

Departments of Psychology and Computer Science
Stanford University
Stanford, CA 94305

Abstract

When can we say that two neural systems are the same? The answer to this question is goal-dependent, and it is often addressed through correlative methods such as Representational Similarity Analysis (RSA) and Centered Kernel Alignment (CKA). What nuances do we miss, however, when we fail to causally probe the representations? Do the dangers of cause vs. correlation exist in comparative representational analyses? In this work, we introduce a method for connecting neural representational similarity to behavior through causal interventions. The method learns orthogonal transformations that find an aligned subspace in which behavioral information from multiple distributed networks' representations can be isolated and interchanged. We first show that the method can be used to transfer the behavior from one frozen Neural Network (NN) to another in a manner similar to model stitching, and we show how the method can complement correlative similarity measures like RSA. We then introduce an efficient subspace orthogonalization technique using the Gram-Schmidt process—that can also be used for Distributed Alignment Search (DAS)—allowing us to perform analyses on larger models. Next, we empirically and theoretically show how our method can be equivalent to model stitching when desired, or it can take a form that is more restrictive to causal information, and in both cases, it reduces the number of required matrices for a comparison of n models from quadratic to linear in n . We then show how we can augment the loss objective with an auxiliary loss to train causally relevant alignments even when we can only read the representations from one of the two networks during training (like with biological networks). Lastly, we use number representations as a case study to explore how our method can be used to compare specific types of representational information across tasks and models.

1 Introduction

An important question for understanding both Artificial and Biological Neural Networks (ANNs and BNNs) is knowing what it means for one distributed system to model or represent another [38]. Establishing isomorphisms between different distributed systems can be useful for simplifying their complexity and for understanding otherwise opaque inner mechanisms. We cannot yet measure from every individual neuron in most BNNs; even if we could, as is the case in ANNs, it is still difficult to find satisfying ways of understanding the neural behavior. Finding simplified models that exhibit the causal relationships of more complex distributed systems can make complex systems more interpretable and communicable, potentially leading to useful insights [4, 5, 34]. Furthermore, there are a number of open questions about how representations differ or converge between architectures, tasks, and modalities [22, 38, 42, 29, 21, 47, 14]. Researchers often use correlational methods to measure the similarity of different neural representations. We can see examples of this in works that perform direct correlational analyses between individual ANN

*Website: grantsrb.github.io - Email: grantsrb@stanford.edu

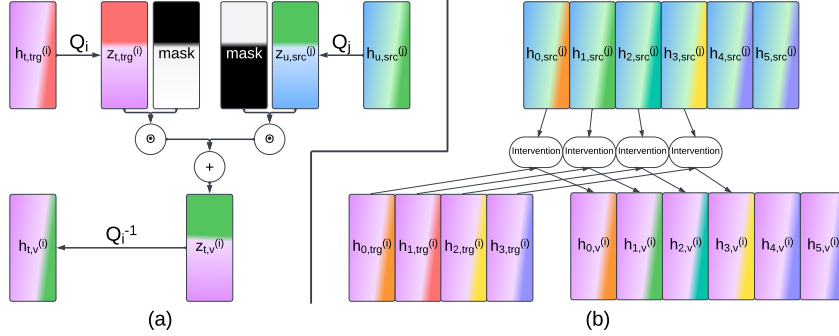


Figure 1: (a) A depiction of an interchange intervention on the target latent vector $h_{t,trg}^{(i)}$ at time t from model ψ_i using the source latent vector $h_{u,src}^{(j)}$ at time u from ψ_j . Rectangles represent vectors; colors depict different types of encoded information. The causally relevant information is spread across the neural population, represented by the red and green semi-vertical slices in the respective h vectors. To disentangle and isolate the causal information, we rotate the h vectors into an aligned space, using Q_i and Q_j , where the relevant information is organized orthogonally to the extraneous information. We can then transfer the relevant information without affecting other types of information by applying binary masks (black represents 0s and white 1s and \odot is a Hadamard product) to the z vectors and taking their sum. We then invert the rotation on $z_{t,v}^{(i)}$ to return it to the original latent space where it can be used by ψ_i . (b) Depicts Stepwise MAS where the individual intervention shown in panel (a) is applied at multiple token positions in the sequence. We limit our interventions to contiguous sets of tokens starting from the first token.

activations and BNN firing rates [45, 30, 23, 44], and in works that use Representational Similarity Analysis (RSA)—or Centered Kernel Alignment (CKA) [24, 43]—finding 2nd order isomorphisms between model and system [25]. We also see examples of this in linear decoding techniques, where linear decodability and predictability can be used as a measure of the type of information encoded in distributed representations [7, 33, 15, 6, 18, 17, 27]. A question remains, however, how to causally associate these neural analyses with behavioral outcomes. What do we miss when we ignore the behavioral relevance of the neural activity [11, 9, 35]?

Some works have made progress toward understanding behavioral representation similarity by transforming intermediate representations from one system into a usable form for a model. We see examples in works like [36] where they attempt to use transformed neural recordings in a trained computational model, and in *model stitching*, where a linear mapping is learned from intermediate representations from one ANN to another for the purpose of measuring similarity or improving one of the two models [26, 31, 2, 28]. To build upon these works, we ask: 1) what do these representational mappings tell us about the underlying representations of the two systems; are behaviorally successful mappings both necessary and sufficient for claims of functional similarity? 2) How can we improve the efficiency of existing methods, and in the process, how can we isolate the behaviorally relevant activity within the representations? 3) How do we achieve causal relevance in systems that we do not have causal access—as is often the case in ANN to BNN comparisons? And 4) How do we isolate the similarity of specific behavioral information in the representations, thus allowing us to compare models with disparate behavioral outputs?

In this work, we introduce a method, Model Alignment Search (MAS), that uses causal interventions to isolate and compare behaviorally relevant activity from neural representations from different ANNs. MAS can be thought of as an efficient form of model stitching [28, 2] or a multi-model extension of Distributed Alignment Search (DAS) [12, 13, 14]—a technique used to align ANNs to directed acyclic graphs. MAS learns a rotation matrix for each model in the comparison with the goal of finding an aligned subspace where behavioral information can be causally interchanged between and within the models. These manipulated representations are then returned back to their original neural space where they are used to produce behavior that can be compared to expected behavior.

The contributions of this work are as follows.

1. We introduce and motivate MAS by comparing to correlative representational similarity methods.
2. We introduce an efficient orthogonal intervention method based on the Gram-Schmidt process that can be used to isolate functional subspaces in both MAS and DAS on large representations.
3. We empirically and theoretically compare MAS to model stitching, showing that it is more efficient when comparing 3 or more models, and it can be more restrictive than model stitching, making it a better choice for some representational analyses.
4. We introduce a *counterfactual latent* auxiliary loss objective that can be used to find behaviorally relevant alignments in cases where one of the two models is causally inaccessible (making the future of the technique relevant for comparisons between ANNs and BNNs).
5. Using numeric cognition as a case study, we show how MAS can be used to examine the similarity of specific types of behavioral information in neural representations.

2 Methods

2.1 Tasks

Each task consists of a sequence of tokens that start with a beginning of sequence token, B, and end with an end of sequence token, E. Some of the tokens in each task are produced by the task environment and define the specific goals within the task. Other tokens are determined by these task provided tokens. Each trial is considered correct when all deterministic tokens are correctly predicted. During the model training, we include all token types in a NTP cross entropy loss, even though many tokens are unpredictable.

Multi-Object Task: The environment presents some number of demonstration (demo) tokens that are each sampled with replacement from the set $\{D_a, D_b, D_c\}$. The task is to produce the same number of response (R) tokens as D tokens and end with an E token. The environment signals the end of the D tokens by producing a trigger (T) token. The number of D tokens at this point is referred to as the *object quantity* for the trial, which is uniformly sampled from 1 to 20 at the beginning. The set of possible tokens includes $\{B, D_a, D_b, D_c, T, R, E\}$. An example sequence with an object quantity of 2 is: "B D_c D_a T R R E"

To prevent solutions that use positional readout [14], we modify the task for transformer trainings: each token in the demo phase has a 0.2 probability of being a "void" token type, V, that has no impact on the object quantity. An example sequence with an object count of 2 could be: "B V D_b V V D_c T R R E". All evaluations and analyses use the original Multi-Object Task.

Same-Object Task: same structure as the Multi-Object task except that all D and R tokens are replaced by a single token type, C. The set of possible tokens includes $\{B, C, T, E\}$. An example sequence with an object quantity of 2 would be: "B C C T C C E".

Modulo: This task is similar to the Multi-Object task except the number of R tokens is equal to the object quantity mod 4. An example trial could be, "B D_b D_c D_a D_c D_b T R E".

Rounding: Similar to the Modulo task except the number of R tokens is equal to the object quantity rounded to the nearest multiple of 3. An example trial could be, "B D_b D_c D_a D_c T R R R E".

2.2 Model Architectures

Each model in this work is autoregressively trained to perform only one of the tasks through NTP. We train 2 model seeds for each task variant up to $> 99.99\%$ accuracy on both training and validation data and freeze the weights before analysis and interpretation. We consider Gated Recurrent Units (GRUs) [8], Long-Short Term Memory recurrent networks (LSTMs) [20], and two layer Transformers based on the Roformer architecture [40, 39, 37]. We also include one analysis using DeepSeek R1 Distill Llama 8B [16]. The custom GRUs and Transformers use a dimensionality of 128, whereas the LSTM uses 64 dimensions for each the h and c vectors. We leave details of GRU and LSTM cells to

the referenced papers beyond noting that the GRU and LSTM based models have the structure:

$$h_{t+1} = f(h_t, x_t) \quad (1)$$

$$\hat{x}_{t+1} = g(h_{t+1}) \quad (2)$$

Where h_t is the hidden state vector at step t , x_t is the input token at step t , f is the recurrent function (either a GRU or LSTM cell), and g is a two layer (two matrix) feed-forward network (FFN) used to make a prediction, \hat{x}_{t+1} , of the token at step $t+1$ from the updated hidden state h_{t+1} .

The transformer architecture uses Rotary Positional Encodings (RoPE) [37] and GELU nonlinearities [19]. Transformers use a history of input tokens, $X_t = [x_1, x_2, \dots, x_t]$, at each time step, t , to make a prediction: $\hat{x}_{t+1} = f(X_t)$, where f is now the transformer architecture. We show results from 2 layer, single attention head transformers. We refer readers to Figure 4 for more details. See training details in Appendix A.1. We sometimes refer to the NNs generally as ψ .

2.3 MAS Formulation

MAS can be thought of as an efficient form of model stitching [28, 2] or a multi-model extension of DAS [12, 13]. In the former case, both stitching and MAS learn a mapping from the representations of one trained model to another. In the latter case, both DAS and MAS attempt to find a causally relevant subspaces in the representations that align with the variables from Directed Acyclic Graphs (DAGs). MAS further measures the degree to which the models’ aligned subspaces align with each other. All analyses are performed on trained NNs with $> 99\%$ task accuracy with frozen weights. We note, however, that MAS can theoretically be used to align models that are not fully trained.

DAS tests the assumption that the hidden state, $h^{(i)} \in R^{d_i}$, for a single model ψ_i , can be written as an orthogonal rotation $h^{(i)} = Q_i z^{(i)}$, where $Q_i \in R^{d_i \times d_i}$ is a learned orthonormal matrix, $z^{(i)} \in R^{d_i}$ consists of contiguous subspaces that encode high-level variables from DAGs, and d_i is the size of the hidden state.

$$h^{(i)} = Q_i z^{(i)} = Q_i \begin{bmatrix} \vec{z}_{\text{var}_1} \\ \vec{z}_{\text{var}_2} \\ \dots \\ \vec{z}_{\text{var}_n} \end{bmatrix} \quad (3)$$

Where each $\vec{z}_{\text{var}_k} \in R^{d_{\text{var}_k}}$ is a column vector of length d_{var_k} satisfying the relation $\sum_{k=1}^n d_{\text{var}_k} = d_i$. The benefit of this alignment is that it allows us understand ψ_i ’s neural activity in terms of interpretable variables by allowing us to isolate and causally manipulate the value of each var_k within the NN’s latent representations. MAS builds on DAS by measuring the degree to which ψ_1 and ψ_2 share the same \vec{z}_{var_k} values for a given var_k . With this formulation, we can freely isolate and manipulate \vec{z}_{var_k} encoded in $h^{(i)}$ using a causal intervention:

$$h_v^{(i)} = Q_i^{-1}((1 - D_{i,\text{var}_k})Q_i h_{\text{trg}}^{(i)} + D_{j,\text{var}_k} Q_j h_{\text{src}}^{(j)}) \quad (4)$$

Where i and j can take on any model index in the set of all models considered, Q_i is a scaled orthogonal rotation matrix for ψ_i , $D_{i,\text{var}_k} \in R^{d_i \times d_i}$ is a diagonal, binary matrix with d_{var_k} non-zero elements used to isolate the dimensions corresponding to \vec{z}_{var_k} , $h_{\text{src}}^{(j)}$ is the *source vector* from which the subspace is harvested, $h_{\text{trg}}^{(i)}$ is the *target vector* into which activity is substituted, and $h_v^{(i)}$ is the resulting intervened vector that then replaces $h_{\text{trg}}^{(i)}$ in the target ψ_i ’s processing, allowing the model to make causally intervened predictions. See Figure 1 for a visualization. In this work, we train Q_i as the product $s_i U_i$ where s_i is a learned scalar and U_i is an orthonormal matrix.

Model stitching can be unified with DAS/MAS by considering a DAG where we assume that all behaviorally relevant information is encoded as a single variable, \vec{z}_{full} , and all extraneous, irrelevant information is encoded in a subspace \vec{z}_{extra} . In this case, $z^{(i)} = \begin{bmatrix} \vec{z}_{\text{full}} \\ \vec{z}_{\text{extra}} \end{bmatrix}$, and we can freely isolate and intervene upon \vec{z}_{full} using Equation 4 once we have learned each Q_i for each $D_{i,\text{full}}$ for each ψ_i .

2.4 MAS Training

MAS relies on the notion of counterfactual behavior to create intervention data to train and evaluate each Q_i . For a given DAG, we know what the DAG’s behavior will be after changing the value of

one of its variables. The counterfactual behavior of the DAG is the resulting behavior of the DAG after changing a specific variable and keeping all other variables and aspects of the task unchanged. This counterfactual behavior can be used as a training signal for Q_i using a standard Next-Token Prediction (NTP) autoregressive loss. Q_i can equivalently learn any permutation of the subspaces in z_i , thus we can restrict our trainings to diagonal matrices D_{i,var_k} that have contiguous, non-zero entries. It is then possible to treat d_{var_k} as a hyperparameter in independent trainings, selecting the Q_i , D_{i,var_k} pair with the best evaluation. Unless otherwise stated, we use values of d_{var} from the better performing of 16 or 32, and we perform our causal interventions on individual time steps in the token sequences. We run the target model ψ_i up a sampled timestep t on the target sequence, using its latent representation at that point as the target vector, $h_{t,\text{trg}}^{(i)}$. We do the same on the source model ψ_j to obtain the source vector, $h_{u,\text{src}}^{(j)}$, at timestep u from a separate source sequence. We then construct $h_{t,v}^{(i)}$ using Equation 4. ψ_i then continues its predictions starting from time t , using $h_{t,v}^{(i)}$ in place of $h_{t,\text{trg}}^{(i)}$. We perform batch gradient descent on Q_1 and Q_2 using the loss as follows for a single counterfactual sequence, k , of length S_k using i as the target model index and $p_{\theta_i}(x_s)$ as the probability generated by ψ_i for the counterfactual token label at step s with N samples in the batch:

$$\mathcal{L}_i^{(k)}(Q_i, Q_j) = -\frac{1}{S_k} \sum_{s=t}^{S_k} \log p_{\theta_i}(x_s^{(k)} | x_{<s}^{(k)}, h_{t,v}^{(k),(i)}) \quad (5)$$

$$\mathcal{L}_{\text{tot}} = \sum_{i=1}^2 \sum_{j=1}^2 \frac{1}{N} \sum_{k=1}^N \mathcal{L}_i^{(k)}(Q_i, Q_j) \quad (6)$$

For the LSTM architecture, we perform MAS on a concatenation of the h and c recurrent state vectors [20]. In the GRUs, we operate on the recurrent hidden state. In the transformers, we operate on the residual stream following the first transformer layer (referred to as the Layer 1 Hidden States in Supplementary Figure 4). Unless otherwise stated, we uniformly sample intervention time points, t and u , from sequence positions containing demo tokens or response tokens (excluding B, T, and E tokens). Unless otherwise stated, we orthogonalize the rotation matrix using PyTorch’s default orthogonalization that uses the exponential of a skew symmetric matrix. See Appendix A.2 for more detail.

MAS Evaluation: We can evaluate the quality of Q_1 and Q_2 using the accuracy of each model’s predictions on counterfactual outputs from held out intervention data. A trial is correct when all deterministic tokens are predicted correctly using the argmax over logits. Unless otherwise stated, we report the proportion of trials correct for the worst performing causal intervention pairing, (i, j) , as the Interchange Intervention Accuracy (IIA). We calculate error bars as Standard Error over unique model seed pairings using 2 model seeds for each training variant. We include two additional seeds for within training type comparisons.

2.5 Mas Variants

Stepwise MAS: For all input embedding analyses we include a MAS variant that applies Equation 4 to multiple, contiguous time-steps in the target and source sequences from step 0 to u —contrasted to a single time step pair (t, u) . This allows for meaningful transfer of information in anti-Markovian solutions [14]. There is a question of what tokens to use to create each $h_{t,\text{trg}}^{(i)}$ before transfer. We show results where each target token comes from the original target sequence padded by the R token when u exceeds the target sequence length. See Figure 1 for a visualization.

Counterfactual Latent MAS (CLMAS): In some settings we wish to examine systems for which we have neural recordings but no causal access (as is often the case in BNNs). We refer to causally inaccessible models as ψ_{nacs} and accessible models as ψ_{acs} . In these cases, we can only train on the behavior of ψ_{acs} but we can read the representations produced by ψ_{nacs} . In these cases, we can adapt Equation 6 to ignore the behavior of ψ_{nacs} like so:

$$\mathcal{L}_{\text{acs}} = \frac{1}{N} \left(\sum_{k=1}^N \mathcal{L}_{\text{acs}}^{(k)}(Q_{\text{acs}}, Q_{\text{nacs}}) + \sum_{k=1}^N \mathcal{L}_{\text{acs}}^{(k)}(Q_{\text{acs}}, Q_{\text{acs}}) \right) \quad (7)$$

We will show that if we merely adapt MAS to train on ψ_{acs} ’s behavior, the resulting Q_{acs} and Q_{nacs} do not achieve high IIA when performing causal interventions on ψ_{nacs} . To address this,

we introduce an auxiliary loss function for the one-directional trainings. The auxiliary objective relies on *Counterfactual Latent (CL) vectors*, which we define as vectors that encode the causal variables that we would expect to exist in the intervened vector, $h_{trg,t}^{(nacs)}$ from Equation 4, following a causal intervention. We can obtain CL vectors by searching through a prerecorded h^{nacs} dataset for situations and behaviors that are consistent with the information we wish to be encoded from the causal intervention. For example, if we have a DAG with variables var_y , var_w , and var_{extra} , and following a causal intervention we expect $h_{t,v}^{(nacs)}$ to have a value of y for variable var_y and w for variable var_w , then the CL vector can be obtained from a pre-recorded representation $h_{CL}^{(nacs)}$ that has the same expected variable values: $var_y = y$ and $var_w = w$. The auxiliary loss $\mathcal{X}^{(k)}$ for a single intervention sample k is composed of an L2 loss and a cosine loss using CL vectors as the ground truth:

$$\mathcal{X}_{L2}^{(k)} = \frac{1}{2} \|h_{t,v}^{(k),(nacs)} - h_{CL}^{(k),(nacs)}\|_2^2 \quad (8)$$

$$\mathcal{X}_{cos}^{(k)} = -\frac{1}{2} \frac{h_{t,v}^{(k),(nacs)} \cdot h_{CL}^{(k),(nacs)}}{\|h_{t,v}^{(k),(nacs)}\|_2 \|h_{CL}^{(k),(nacs)}\|_2} \quad (9)$$

where $h_{t,v}^{(nacs)}$ is the intervened target vector for the causally inaccessible model, and k denotes the index of the sample within the batch. The total CLMAS training loss is a weighted sum of the loss from Equation 7 and the auxiliary loss where λ is a hyperparameter: $\mathcal{L}_{CMAS} = \lambda(\mathcal{X}_{L2} + \mathcal{X}_{cos}) + (1 - \lambda)\mathcal{L}_{acs}$

Transferring Specific Variables Through our choice of counterfactual training behavior, we can explore alignment of specific types of representations between models. We use representations of number as a case study for their precise but general nature. To do this, we construct counterfactual sequences based on the assumption that the numeric information in h_{src} is transferred to h_{trg} and all other information is left unaffected. We assume that the models encode a single numeric variable in the Multi-Object, Same-Object, Modulo , and Rounding tasks [14]. In the arithmetic task, we assume there is a numeric representation for the number of remaining operations, **Rem Ops**, and another representation for the cumulative value, **Cumu Val**. See expanded details in Appendix A.7.

Model Stitching: As baselines, we include causal intervention methods that we refer to as **Latent Stitch** and **Stitch**. Latent Stitch consists of a single orthogonal matrix Q that learns to map $h_{u,src}^{(k),(acs)}$ to $h_{CL}^{(k),(nacs)}$ by minimizing the CL auxiliary loss from Equation 8 without the Equation 7 objective. Stitch consists of a single, possibly low rank, orthogonal matrix Q trained in a single behavioral direction from ψ_{nacs} to ψ_{acs} without the CL auxiliary loss. Unless otherwise stated assume Q is full rank and the IIA is reported from validation interventions in the trained direction, from ψ_{nacs} to ψ_{acs} .

2.6 Gram-Schmidt Alignment Matrices

To save compute for analyses on large vectors, we present an intervention method that only learns the components specific to the subspace of interest. If we assume the number of dimensions in the aligned space is n , we can use the Gram-Schmidt process to orthogonalize and train only n components of an orthogonal matrix for ψ_i . To do this, n column vectors $v_k \in R^{d_i}$ are sampled from a normal distribution where d_i is the latent dimensionality of ψ_i . We can then make an orthogonal set of vectors $u_k \in R^{d_i}$, and thus a partial orthogonal matrix $Q \in R^{m \times n}$, by subtracting out the projections of all preceding components from each v_i where $u_1 = v_1$:

$$\text{proj}_u(v) = \frac{u^\top v}{u^\top u} u \quad (10)$$

$$u_k = v_k - \sum_{i=1}^{k-1} \text{proj}_{u_i}(v_k) \quad (11)$$

$$Q = \begin{bmatrix} \frac{u_1}{\|u_1\|} & \frac{u_2}{\|u_2\|} & \dots & \frac{u_n}{\|u_n\|} \end{bmatrix} \quad (12)$$

Using partial rotation matrices Q_i and Q_j for ψ_i and ψ_j , we can formulate a MAS (or DAS) intervention as follows (see Appendix A.8 for proof of Equation 13):

$$h_{v,t}^{(i)} = h_{trg,t}^{(i)} + Q_i(-Q_i^\top h_{trg,t}^{(i)} + Q_j^\top h_{src,u}^{(j)}) \quad (13)$$

2.7 Representational Similarity Analysis (RSA)

For a given model layer, we run the model on a batch of sequences consisting of 15 sequences from each object quantity 1-20. We then sample 1000 representational vectors uniformly from all time points excluding padding and end of sequence tokens. We construct a Representational Dissimilarity Matrix (RDM) as 1 minus the cosine similarity matrix over each pair-wise comparison of the representations (resulting in an RDM of dimensions 1000×1000). We create an RDM for two models and compare the RDMs using Spearman’s rank correlation on the lower triangle of each matrix [41]. We perform the RDM sampling 10 times and report the average over all 10 correlations. See Appendix A.4 for CKA methods.

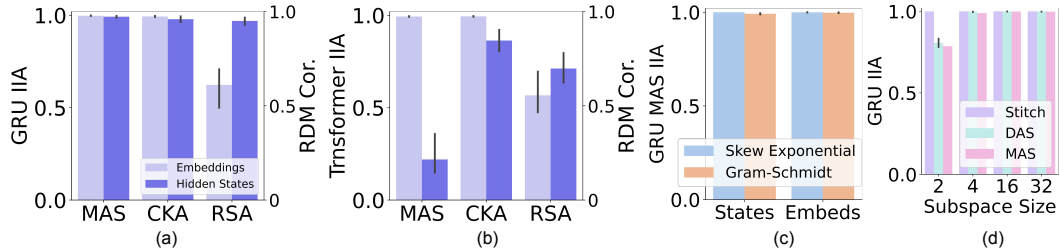


Figure 2: **(a) and (b)** A comparison of MAS on the left axes and CKA and RSA on the right axes. We examine both the input embeddings and the hidden state vectors for models trained on the Multi-Object task. (a) Results for GRUs, where RSA can give low estimates of similarity whereas MAS shows high causal transfer as we might expect. (b) Results for 2-layer Transformers where we see a similar effect as (a) in the embeddings and we see a potential over-estimation of similarity of the hidden states in CKA and RSA due to the fact that prior work has shown the transformers to resolve the counting task at each step in the sequence [14] (as reflected in the low MAS IIA). **(c)** A demonstration on Multi-Object GRUs of the reasonable performance of the Gram-Schmidt causal interventions introduced in Equation 13 relative to the default exponentiated skew symmetric matrix interventions from Equation 4. **(d)** Comparison of the IIA from DAS and MAS for different sizes of the aligned subspace, and model stitching with different rank transformation matrices.

3 Results

3.1 The Importance of Causal Analyses

We first set out to demonstrate reasons why MAS could be preferable to a correlative similarity method such as RSA. RSA and CKA are second order correlational methods that examine the similarity between sample correlation matrices constructed from two models’ representations (see Appendix A.3 for details). We provide comparisons between models differing only by seed to ground our intuition for MAS, RSA, and CKA values. Turning our attention to Figure 2(a) we see that MAS can successfully align the behavior between GRUs trained on the Multi-Object task, both within the embedding and hidden state layers. RSA, however, shows a low RDM correlation on the embedding layer relative to its value for the hidden state layer². A similar issue occurs in Figure 2(b) where we see that Multi-Object Transformers exhibit the same RSA embedding issue, and the hidden states have potentially unintuitive values for both CKA and RSA. Prior work has shown that Transformers use an anti-Markovian solution that recomputes the relevant numeric information at each step in the Multi-Object task, thus the low MAS result for the hidden states is to be expected [14, 3]. These sorts of anti-Markovian solutions are easily missed from correlative methods such as RSA and CKA. Furthermore, it is difficult to interpret the CKA and RSA results as we might expect them to be higher for the same model architecture trained on different seeds. We use this result to highlight the potential importance of supplementing correlative methods with causal counterparts. We note that questions on how to interpret RSA values have been addressed in previous works [25, 38, 10].

²When comparing the same RDMs using Pearson correlation, the values return to near ceiling, indicating that the issue is in part due to the way that the Spearman’s Rank handles RDMs with different relative extrema.

3.2 Gram-Schmidt Alignment Results

We show the Gram-Schmidt alignment method used on the hidden states and embeddings in the Multi-Object GRUs in Figure 2. We can see that the results are comparable to the standard orthogonalization method that uses the exponential of a skew symmetric matrix [32]. Motivated by this result, we further examined the new orthogonalization method by performing MAS between the embeddings of the Multi-Object GRUs and Transformers, the GRUs and LSTMs, and the Transformers and LSTMs, each achieving similar IIAs of >0.99 . We compared these GRUs to the Same-Object GRUs as a baseline, achieving 0.555, as expected. Lastly, we used the method to perform a MAS analysis between the embedding layer of one of the Multi-Object GRUs with the embeddings of DeepSeek R1 Distill LLaMA 8B. The DeepSeek model performed an in-context version of the Multi-Object task using the token for "nut" as the demonstration tokens and "seed" as response tokens (see Appendix A.5 for further detail). We used a subspace size equal to the full dimensionality of the GRU and achieved an IIA of 0.400.

3.3 MAS is an Efficient, Restrictive Form of Model Stitching

We first note that while traditional model stitching learns a transformation matrix for each pair of models, MAS learns a single transformation matrix for each model in the alignment [28, 2]. This reduces the number of matrices required for comparing n models from $n(n - 1)$ when training the traditional model stitching using behavior, or $\binom{n}{2}$ when solving an invertible Procrustes mapping between representations, to n when using MAS. Furthermore, when aligning the full dimensionality of the latent vectors, the trained MAS matrices can be combined to become equivalent to model stitching.

Now turning to Figure 2(d), we compare the IIA of MAS, DAS, and model stitching in the Multi-Object GRU models. The x-axis of the panel shows the aligned subspace size for DAS and MAS, and shows the rank of the transformation matrix for stitching. We report the IIA of the worst performing intervention direction for MAS, the only direction for DAS, and the trained direction for stitching. We see that the models' behavior can be compressed to as few as 4 dimensions when using DAS and MAS, and these methods have comparable IIAs. Stitching, however, has nearly perfect performance even for rank 2 trainings.

To better understand this result, we first formulate model stitching in terms of the latent states, h , and the interpretable z vectors. Causal interventions can be thought of as an equality constraint, where elements that are exchanged have some functional equivalence for successful interventions. Thus, traditional stitching is similar to learning a matrix $W \in \mathbb{R}^{d_1 \times d_2}$ such that $h^{(1)} = Wh^{(2)}$. We can rewrite this as follows:

$$h^{(1)} = Q_1 z^{(1)} = Wh^{(2)} = WQ_2 z^{(2)} \quad (14)$$

$$z^{(1)} = Q_1^{-1} WQ_2 z^{(2)} = X z^{(2)} \quad (15)$$

If we focus on only a single variable component, var_1 , in $z^{(1)}$, and assume it is only 1 dimensional for notational simplicity, we can see that $\vec{z}_{var_1} = \sum_{k=1}^{d_2} x_{1,k} z_k^{(2)}$ where the $x_{1,col}$ are elements of the first row of X and $z_k^{(2)}$ are row elements of $z^{(2)}$. This shows that \vec{z}_{var_1} can include non-causal elements from $z^{(2)}$ in the direct model-stitching case. Furthermore, we note that because stitching completely replaces the target vector with the transformed source vector, the mapping only needs to learn a single sufficient causal representation for each behavioral outcome.

Using the same functional equivalence formulation for MAS, we see that MAS finds mappings such that for the causal variable of focus, var_1 , $\vec{z}_{var_1}^{(1)} = \vec{z}_{var_1}^{(2)}$ demonstrated as follows:

$$D_{var_1} Q_1 h^{(1)} = D_{var_1} z^{(1)} = \begin{bmatrix} \vec{z}_{var_1}^{(1)} \\ \mathbf{0} \end{bmatrix} = \begin{bmatrix} \vec{z}_{var_1}^{(2)} \\ \mathbf{0} \end{bmatrix} = D_{var_1} z^{(2)} = D_{var_1} Q_2 h^{(2)} \quad (16)$$

We use this to suggest that MAS is a more causally focused choice than typical model stitching for addressing questions of how behaviorally relevant information is encoded in different neural systems.

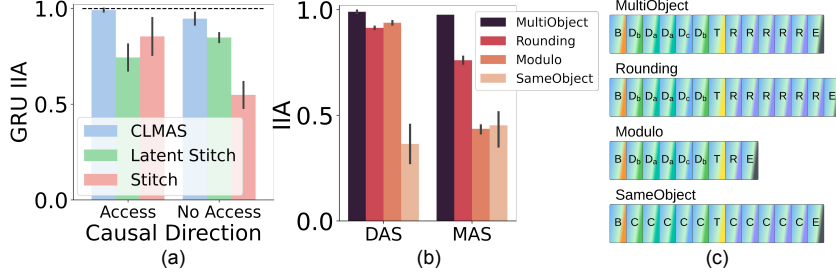


Figure 3: **(a)** Comparison of the IIA for CLMAS, Latent Stitching, and behavioral Stitching in different intervention directions on the Multi-Object GRU models. The dashed line indicates MAS IIA. *Access* refers to causal interventions from the inaccessible ϕ_{nacs} as the source, to the accessible ϕ_{acs} as the target (this direction is included in the CLMAS, MAS, and Stitch training data). *No Access* refers to validation interventions using ϕ_{acs} as the source and ϕ_{nacs} as the target. We see that CLMAS has the best performance recovery while also providing the best performance using ϕ_{acs} as the target. **(b)** An methods comparison of the transferrability of the behaviorally relevant numeric information between the Multi-Object GRU models and the Multi-Object, Rounding, Modulo, and Same-Object models. We take the average of Stitching trained in both directions. DAS shows the expected performance when ϕ_1 and ϕ_2 represent numbers the same way. The inflated Stitching results are potentially explained by less restriction on their ability to use non-behavioral information in their mapping (see Section 3.3). **(c)** Example token sequences of the GRU tasks from panel (b).

3.4 Providing Greater Causal Relevance with CLMAS

We can see from Figure 3 the results of CLMAS compared to behavioral model stitching (Stitch) and latent model stitching (Latent Stitch). It is important to note that the Latent Stitch, Stitch, and CLMAS variants do not include the autoregressive training signal in the *No Access* causal direction. The MAS performance provides a theoretic upper bound on the possible IIA for CLMAS, shown by the dashed black line. Stitching provides a lower bound on the possible CLMAS performance in the *No Access* direction. Lastly, Latent Stitch—which trains a rotation matrix to map latent vectors from the accessible ϕ_{acs} to latent vectors of the inaccessible ϕ_{nacs} in the absence of behavioral training—provides a baseline of existing methods. We see that CLMAS recovers more of the possible performance of MAS than the Latent Stitch. This demonstrates the potential of CLMAS to recover causally relevant intervention rotation matrices even when we do not have causal access to one of the models in the comparison.

3.5 MAS Can Answer Questions About Specific Causal Information

Turning our attention to Figure 3(b), we first note that these results demonstrate a causal comparison of the types of numeric representations in GRUs trained on different numeric tasks. We see from the DAS IIA that we can align the Multi-Object, Rounding, and Modulo GRUs to DAGs that use individual numeric variables. We then use MAS to show that the numeric representations differ across the GRUs. We do a further exploration on an arithmetic task in Appendix A.6.

4 Limitations/Future Directions

The tasks and models we use in this work are simplistic and contrived, but their purpose is to serve as a proof of principle for the MAS methodology, and to prove points about the importance of restricted causal methods. We offer RSA, model stitching, and DAS results as a grounding for the MAS results, reducing the importance of the task complexity. Furthermore, MAS does not offer guarantees for the complete removal of non-functional neural activity when performing interventions. We attempt to mitigate this issue by finding low dimensional subspaces for the interventions. We point out, however, that MAS is better than previous methods in this respect.

Despite CLMAS’s successes, there is an obvious difficulty of evaluating the causal relevance of the learned alignment function without possessing causal access to the inaccessible model. This makes CLMAS largely irrelevant for isolating functional information without also causally testing on the

BNN of interest. We note, however, that CLMAS still can provide value in biological settings as the method can potentially reduce or remove the need for stimulation during the alignment training. Concretely, one could record from the BNN, then perform the CLMAS trainings, and then only use the stimulation to evaluate the effectiveness of the alignment.

Acknowledgments and Disclosure of Funding

Thank you to the PDP Lab and the Stanford Psychology department for funding. Thank you to Stephen Baccus, Noah Goodman, Zen Wu, Atticus Geiger, Linas Nasvytis, Jenelle Feather, Chris Potts, Alexa Tartaglini, Daniel Wurgaf, the PDP lab, and the Stanford Mech Interp community for thoughtful discussion. Thanks to Joshua Melander, Josh Wilson, Ben Prystawski, Jerome Han, and Andrew Lampinen for thoughtful discussion and feedback. Special thanks to my advisor Jay McClelland for support, encouragement, feedback, and many thoughtful conversations.

References

- [1] Jimmy Lei Ba, Jamie Ryan Kiros, and Geoffrey E. Hinton. Layer normalization, 2016.
- [2] Yamini Bansal, Preetum Nakkiran, and Boaz Barak. Revisiting model stitching to compare neural representations, 2021.
- [3] Freya Behrens, Luca Biggio, and Lenka Zdeborová. Counting in small transformers: The delicate interplay between attention and feed-forward layers, 2024.
- [4] Rosa Cao and Daniel Yamins. Explanatory models in neuroscience: Part 1 – taking mechanistic abstraction seriously, April 2021. arXiv:2104.01490 [cs, q-bio].
- [5] Rosa Cao and Daniel Yamins. Explanatory models in neuroscience, Part 2: Functional intelligibility and the contravariance principle. *Cognitive Systems Research*, 85:101200, June 2024.
- [6] Mathilde Caron, Hugo Touvron, Ishan Misra, Hervé Jégou, Julien Mairal, Piotr Bojanowski, and Armand Joulin. Emerging properties in self-supervised vision transformers, 2021.
- [7] Ting Chen, Simon Kornblith, Mohammad Norouzi, and Geoffrey Hinton. A simple framework for contrastive learning of visual representations. *ICML*, 2020.
- [8] Kyunghyun Cho, Bart van Merriënboer, Çağlar Gülcehre, Fethi Bougares, Holger Schwenk, and Yoshua Bengio. Learning phrase representations using RNN encoder-decoder for statistical machine translation. *CoRR*, abs/1406.1078, 2014.
- [9] Nathan Cloos, Moufan Li, Markus Siegel, Scott L. Brincat, Earl K. Miller, Guangyu Robert Yang, and Christopher J. Cueva. Differentiable optimization of similarity scores between models and brains, 2024.
- [10] Marin Dujmović, Jeffrey S Bowers, Federico Adolfi, and Gaurav Malhotra. The pitfalls of measuring representational similarity using representational similarity analysis. *bioRxiv*, 2022.
- [11] Atticus Geiger, Duligur Ibeling, Amir Zur, Maheep Chaudhary, Sonakshi Chauhan, Jing Huang, Aryaman Arora, Zhengxuan Wu, Noah Goodman, Christopher Potts, and Thomas Icard. Causal abstraction: A theoretical foundation for mechanistic interpretability, 2024.
- [12] Atticus Geiger, Hanson Lu, Thomas Icard, and Christopher Potts. Causal abstractions of neural networks. *CoRR*, abs/2106.02997, 2021.
- [13] Atticus Geiger, Zhengxuan Wu, Christopher Potts, Thomas Icard, and Noah D. Goodman. Finding alignments between interpretable causal variables and distributed neural representations, 2023.
- [14] Satchel Grant, Noah D. Goodman, and James L. McClelland. Emergent symbol-like number variables in artificial neural networks, 2024.

[15] Jean-Bastien Grill, Florian Strub, Florent Altché, Corentin Tallec, Pierre H. Richemond, Elena Buchatskaya, Carl Doersch, Bernardo Avila Pires, Zhaohan Daniel Guo, Mohammad Gheshlaghi Azar, Bilal Piot, Koray Kavukcuoglu, Rémi Munos, and Michal Valko. Bootstrap your own latent: A new approach to self-supervised learning, 2020.

[16] Daya Guo, Dejian Yang, Haowei Zhang, Junxiao Song, Ruoyu Zhang, Runxin Xu, Qihao Zhu, Shirong Ma, Peiyi Wang, Xiao Bi, et al. Deepseek-r1: Incentivizing reasoning capability in llms via reinforcement learning. *arXiv preprint arXiv:2501.12948*, 2025.

[17] James V Haxby. Multivariate pattern analysis of fMRI: Parcellating abstract from concrete representations. *NEuroimage*, 62(2):2013, 2013.

[18] James V. Haxby, M. Ida Gobbini, Maura L. Furey, Alumit Ishai, Jennifer L. Schouten, and Pietro Pietrini. Distributed and overlapping representations of faces and objects in ventral temporal cortex. *Social Neuroscience: Key Readings*, 293(September):87–96, 2001.

[19] Dan Hendrycks and Kevin Gimpel. Gaussian error linear units (gelus), 2023.

[20] Sepp Hochreiter and Jürgen Schmidhuber. Long short-term memory. *Neural Computation*, 9(8):1735–1780, 11 1997.

[21] Eghbal Hosseini, Colton Casto, Noga Zaslavsky, Colin Conwell, Mark Richardson, and Evelina Fedorenko. Universality of representation in biological and artificial neural networks. *bioRxiv*, 2024.

[22] Minyoung Huh, Brian Cheung, Tongzhou Wang, and Phillip Isola. The platonic representation hypothesis, 2024.

[23] Meenakshi Khosla and Alex H. Williams. Soft matching distance: A metric on neural representations that captures single-neuron tuning, 2023.

[24] Simon Kornblith, Mohammad Norouzi, Honglak Lee, and Geoffrey Hinton. Similarity of neural network representations revisited, 2019.

[25] Nikolaus Kriegeskorte, Marieke Mur, and Peter Bandettini. Representational similarity analysis - connecting the branches of systems neuroscience. *Frontiers in Systems Neuroscience*, 2, 2008.

[26] Zorah Lähner and Michael Moeller. On the direct alignment of latent spaces. In Marco Fumero, Emanuele Rodolá, Clementine Domine, Francesco Locatello, Karolina Dziugaite, and Caron Mathilde, editors, *Proceedings of UniReps: the First Workshop on Unifying Representations in Neural Models*, volume 243 of *Proceedings of Machine Learning Research*, pages 158–169. PMLR, 15 Dec 2024.

[27] Andrew Kyle Lampinen, Stephanie CY Chan, and Katherine Hermann. Learned feature representations are biased by complexity, learning order, position, and more. *arXiv preprint arXiv:2405.05847*, 2024.

[28] Karel Lenc and Andrea Vedaldi. Understanding image representations by measuring their equivariance and equivalence, 2015.

[29] Jiaang Li, Yova Kementchedjhieva, Constanza Fierro, and Anders Søgaard. Do Vision and Language Models Share Concepts? A Vector Space Alignment Study. *Transactions of the Association for Computational Linguistics*, 12:1232–1249, September 2024.

[30] Niru Maheswaranathan, Lane T. McIntosh, Hidenori Tanaka, Satchel Grant, David B. Kastner, Josh B. Melander, Aran Nayebi, Luke Brezovec, Julia Wang, Surya Ganguli, and Stephen A. Baccus. The dynamic neural code of the retina for natural scenes. *bioRxiv*, 2019.

[31] Luca Moschella, Valentino Maiorca, Marco Fumero, Antonio Norelli, Francesco Locatello, and Emanuele Rodolà. Relative representations enable zero-shot latent space communication, March 2023. *arXiv:2209.15430 [cs]*.

[32] Adam Paszke, Sam Gross, Francisco Massa, Adam Lerer, James Bradbury, Gregory Chanan, Trevor Killeen, Zeming Lin, Natalia Gimelshein, Luca Antiga, Alban Desmaison, Andreas Köpf, Edward Z. Yang, Zach DeVito, Martin Raison, Alykhan Tejani, Sasank Chilamkurthy, Benoit Steiner, Lu Fang, Junjie Bai, and Soumith Chintala. Pytorch: An imperative style, high-performance deep learning library. *CoRR*, abs/1912.01703, 2019.

[33] Alec Radford, Jong Wook Kim, Chris Hallacy, Aditya Ramesh, Gabriel Goh, Sandhini Agarwal, Girish Sastry, Amanda Askell, Pamela Mishkin, Jack Clark, Gretchen Krueger, and Ilya Sutskever. Learning transferable visual models from natural language supervision, 2021.

[34] Blake A. Richards, Timothy P. Lillicrap, Philippe Beaudoin, Yoshua Bengio, Rafal Bogacz, Amelia Christensen, Claudia Clopath, Rui Ponte Costa, Archy de Berker, Surya Ganguli, Colleen J. Gillon, Danijar Hafner, Adam Kepecs, Nikolaus Kriegeskorte, Peter Latham, Grace W. Lindsay, Kenneth D. Miller, Richard Naud, Christopher C. Pack, Panayiota Poirazi, Pieter Roelfsema, João Sacramento, Andrew Saxe, Benjamin Scellier, Anna C. Schapiro, Walter Senn, Greg Wayne, Daniel Yamins, Friedemann Zenke, Joel Zylberberg, Denis Therien, and Konrad P. Kording. A deep learning framework for neuroscience. *Nature Neuroscience*, 22(11):1761–1770, November 2019. Publisher: Nature Publishing Group.

[35] Rylan Schaeffer, Mikail Khona, Sarthak Chandra, Mitchell Ostrow, Brando Miranda, and Sanmi Koyejo. Does maximizing neural regression scores teach us about the brain? In *UniReps: 2nd Edition of the Workshop on Unifying Representations in Neural Models*, 2024.

[36] Nicholas J. Sexton and Bradley C. Love. Reassessing hierarchical correspondences between brain and deep networks through direct interface. *Science Advances*, 8(28):eabm2219, July 2022. Publisher: American Association for the Advancement of Science.

[37] Jianlin Su, Yu Lu, Shengfeng Pan, Ahmed Murtadha, Bo Wen, and Yunfeng Liu. Roformer: Enhanced transformer with rotary position embedding, 2023.

[38] Ilia Sucholutsky, Lukas Muttenthaler, Adrian Weller, Andi Peng, Andreea Bobu, Been Kim, Bradley C. Love, Erin Grant, Iris Groen, Jascha Achterberg, Joshua B. Tenenbaum, Katherine M. Collins, Katherine L. Hermann, Kerem Oktar, Klaus Greff, Martin N. Hebart, Nori Jacoby, Qiuyi Zhang, Raja Marjieh, Robert Geirhos, Sherol Chen, Simon Kornblith, Sunayana Rane, Talia Konkle, Thomas P. O’Connell, Thomas Unterthiner, Andrew K. Lampinen, Klaus-Robert Müller, Mariya Toneva, and Thomas L. Griffiths. Getting aligned on representational alignment. *arXiv*, November 2023. arXiv:2310.13018 [cs, q-bio].

[39] Hugo Touvron, Thibaut Lavril, Gautier Izacard, Xavier Martinet, Marie-Anne Lachaux, Timothée Lacroix, Baptiste Rozière, Naman Goyal, Eric Hambro, Faisal Azhar, Aurelien Rodriguez, Armand Joulin, Edouard Grave, and Guillaume Lample. Llama: Open and efficient foundation language models, 2023.

[40] Ashish Vaswani, Noam Shazeer, Niki Parmar, Jakob Uszkoreit, Llion Jones, Aidan N. Gomez, Łukasz Kaiser, and Illia Polosukhin. Attention is all you need. *CoRR*, abs/1706.03762, 2017.

[41] Pauli Virtanen, Ralf Gommers, Travis E. Oliphant, Matt Haberland, Tyler Reddy, David Cournapeau, Evgeni Burovski, Pearu Peterson, Warren Weckesser, Jonathan Bright, Stéfan J. van der Walt, Matthew Brett, Joshua Wilson, K. Jarrod Millman, Nikolay Mayorov, Andrew R. J. Nelson, Eric Jones, Robert Kern, Eric Larson, C J Carey, İlhan Polat, Yu Feng, Eric W. Moore, Jake VanderPlas, Denis Laxalde, Josef Perktold, Robert Cimrman, Ian Henriksen, E. A. Quintero, Charles R. Harris, Anne M. Archibald, Antônio H. Ribeiro, Fabian Pedregosa, Paul van Mulbregt, and SciPy 1.0 Contributors. SciPy 1.0: Fundamental Algorithms for Scientific Computing in Python. *Nature Methods*, 17:261–272, 2020.

[42] Junxuan Wang, Xuyang Ge, Wentao Shu, Qiong Tang, Yunhua Zhou, Zhengfu He, and Xipeng Qiu. Towards Universality: Studying Mechanistic Similarity Across Language Model Architectures, October 2024. arXiv:2410.06672 [cs].

[43] Alex H. Williams. Equivalence between representational similarity analysis, centered kernel alignment, and canonical correlations analysis. *bioRxiv*, 2024.

[44] Alex H. Williams, Erin Kunz, Simon Kornblith, and Scott W. Linderman. Generalized shape metrics on neural representations, 2022.

[45] Daniel L.K. Yamins and James J. DiCarlo. Using goal-driven deep learning models to understand sensory cortex. *Nature Neuroscience*, 19(3):356–365, 2016.

[46] Jerrold H Zar. Spearman rank correlation. *Encyclopedia of Biostatistics*, 7, 2005.

[47] Le Zhang, Qian Yang, and Aishwarya Agrawal. Assessing and learning alignment of unimodal vision and language models, 2024.

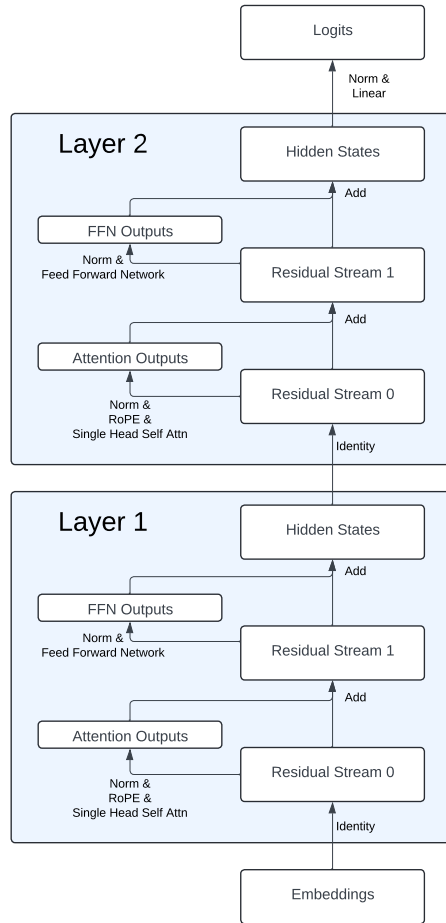


Figure 4: Figure and caption taken from [14]. Diagram of the transformer architecture used in this work. White rectangles represent activation vectors, arrows represent functional operations. All causal interventions were performed on either the Hidden State activations from Layer 1 or the Embeddings layer. All normalizations are Layer Norms [1].

A Appendix

A.1 Model Details

All artificial neural network models were implemented and trained using PyTorch [32] on a single Nvidia Titan X GPU. Unless otherwise stated, all models used an embedding and hidden state size of 128 dimensions. To make the token predictions, each model used a two layer multi-layer perceptron (MLP) with GELU nonlinearities, with a hidden layer size of 4 times the hidden state dimensionality with 50% dropout on the hidden layer. The GRU and LSTM model variants each consisted of a single recurrent cell followed by the output MLP. Unless otherwise stated, the transformer architecture consisted of two layers using Rotary positional encodings [37]. Each model variant used the same learning rate scheduler, which consisted of the original transformer [40] scheduling of warmup followed by decay. We used 100 warmup steps, a maximum learning rate of 0.001, a minimum of 1e-7, and a decay rate of 0.5. We used a batch size of 128, which caused each epoch to consist of 8 gradient update steps.

A.2 MAS (and Associated Variants) Training Details

All MAS trainings were implemented and trained using PyTorch [32] on single Nvidia Titan X GPUs. For each rotation matrix training, we use 10000 intervention samples and 1000 samples for validation and testing. We uniformly sampled corresponding indices upon which to perform interventions, excluding the B, T, and E tokens in the numeric equivalence tasks from possible intervention sample indices. In the Arithmetic task, we used the comma token for Rem Ops and Cumu Val interventions. When intervening upon a state in the demo phase in the numeric equivalence tasks, we uniformly sample a number of steps to continue the demo phase that will keep the object quantity below 20. We orthogonalize the matrices, Q_i , using PyTorch’s orthogonal parametrization with default settings. PyTorch creates the orthogonal matrix as the exponential of a skew symmetric matrix. We train the rotation matrices for 1000 epochs, with a batch size of 512 used for each model index pairing. We only perform experiments considering two models. Each gradient step uses the average gradient over batches of all 4 i, j pairings. We select the checkpoint with the best validation performance for analysis. We use a learning rate of 0.001 and an Adam optimizer.

A.3 RSA Details

We performed RSA on a subsample of a dataset of 15 sampled sequences for each object quantity ranging from 1-20 on the task that each model was trained on for each model. We first ran the models on their respective datasets to collect the latent representations. We sampled 1000 of these latent vectors as the sample representations in a matrix $M_k \in R^{N \times d_k}$ where k refers to the model index, N is the number of latent vectors ($N = 1000$ in our analyses), d_k is the dimensionality of a single latent vector for model k . We then calculated the sample cosine distance matrices (1-cosine similarity) for each model resulting in matrices $C_k \in R^{N \times N}$. Lastly we calculated the Spearman’s Rank Correlation Coefficient between the lower triangles of the matrices C_1 and C_2 as the RSA value using python’s SciPy package [46, 25, 41]. We resampled the 1000 vectors 10 times and recalculated the RSA score 10 times and report the average over these scores.

A.4 CKA Details

We performed CKA on a subsample of a dataset of 15 sampled sequences for each object quantity ranging from 1-20 on the task that each model was trained on for each model. We first ran the models on their respective datasets to collect the latent representations. We sampled 1000 of these latent vectors as the sample representations in a matrix $M_k \in R^{N \times d_k}$ where k refers to the model index, N is the number of latent vectors ($N = 1000$ in our analyses), d_k is the dimensionality of a single latent vector for model k . We then normalized the vectors along the sample dimension by subtracting the mean and dividing by the standard deviation (using d_k means and d_k standard deviations calculated over 1000 samples). Using these samples we calculated the kernel matrices using cosine similarity to create matrices $C_k \in R^{N \times N}$. Using these matrices, we computed the Hilbert-Schmidt Independence Criterion (HSIC) where $I \in R^{N \times N}$ is the identity and $J \in R^{N \times N}$ is a matrix of values all equal to 1:

$$H = I - \frac{1}{N} J \quad (17)$$

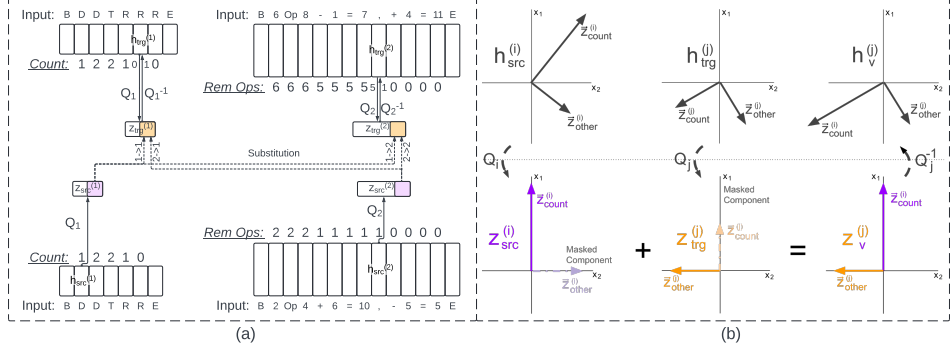


Figure 5: (a) Diagram of MAS between models trained on structurally different tasks. We see all four intervention directions on the latent vectors (rectangles) of a Multi-Object GRU, ψ_1 , and an Arithmetic GRU ψ_2 . The value of the causal variables following each input token are shown above the h_{src} and below the h_{trg} vectors. In the h_{trg} vectors, we see the variable value before and after the intervention to the left and right of the arrows respectively—the Count for ψ_1 and Rem Ops for ψ_2 . The dotted *Substitution* arrows each correspond to a single intervention. The models make predictions using the intervened vector following the intervention. (b) A 2D vector depiction of a hypothetical intervention that substitutes the value of the Count variable from ψ_i , $\vec{z}_{count}^{(1)}$, into the Count variable, $\vec{z}_{count}^{(2)}$ in ψ_j where the superscripts refer to the originating model. Using learned matrices Q_1 and Q_2 , $h_{src}^{(1)}$ and $h_{trg}^{(2)}$ are rotated into $z_{src}^{(1)}$ and $z_{trg}^{(2)}$ where the \vec{z}_{count} subspace is organized into a contiguous subset of vector dimensions disentangled from all other information. In this aligned space the \vec{z}_{count} values can be freely exchanged without affecting other information. Lastly, $z_v^{(2)}$ is returned to ψ_2 's hidden state space by inverting Q_2 and is used for inference by ψ_2 .

$$\text{HSIC}(C_1, C_2) = \frac{\text{trace}(C_1 H C_2 H)}{(N-1)^2} \quad (18)$$

and lastly we computed CKA as the following:

$$\text{CKA} = \frac{\text{HSIC}(C_1, C_2)}{\sqrt{\text{HSIC}(C_1, C_1)\text{HSIC}(C_2, C_2)}} \quad (19)$$

[24]. We resampled the 1000 vectors 10 times and recalculated the CKA score 10 times and report the average over these scores.

A.5 DeepSeek

To avoid fine-tuning the DeepSeek model, we prompted the model to perform a numeric equivalence task similar to the Multi-Object task. The prompt consisted of: "" User: For each trial, I am going to say "nut" some number of times and then I want you to respond by saying "seed" the exact same number of times that I said "nut" in that trial. Please say "stop" at the end of your response to indicate that you are finished. Do not say or think anything else. Example: User: nut : seed stop Example: User: nut nut : seed seed stop Begin Trial: User: "" Following the prompt, we provided some number of "nut" tokens and considered a trial correct when DeepSeek responded with the correct number of "seed" tokens followed by the "stop" token. DeepSeek was only successful on counts up to 12, so the MAS analysis only included values from 1-12.

A.6 Arithmetic

To further explore how representations of number differ across tasks, we include a comparison between GRUs trained on the Multi-Object task and an arithmetic task. See Figure 5 for a visual of MAS applied between the Arithmetic and Multi-Object tasks.

Arithmetic Task: This task consists of an indication of the number of addition/subtraction operations, an initial value, and then the operations interlaced with the cumulative value (cumu val) of the operations. An example sequence is: "B 3 4 + 3 = 7 , + 11 = 18 , - 5 = 13 E", where the first number

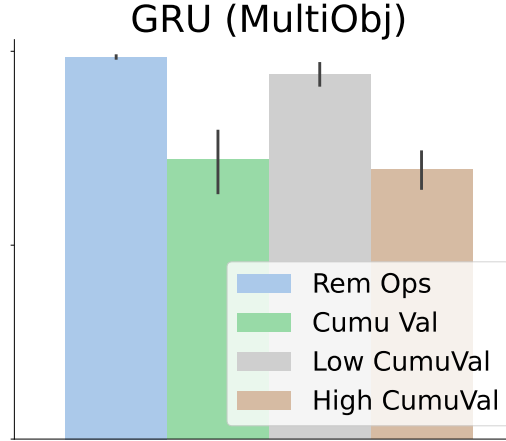


Figure 6: MAS used to compare the Count variable from the Multi-Object GRUs to the Rem Ops and Cumu Val variables from the Arithmetic GRUs. Cumu Val results are from MAS trained with all possible Cumu Val values. Low Cumu Val results are from a separate MAS analysis restricted to Cumu Val values of 1-10, same as the range of Rem Ops variable. High Cumu Val results are from MAS conditioned on values from 11-20.

indicates the number of operations in the trial. The 2nd number is a sampled start value. Each operand is a sampled value that is combined with the cumu val according to the operator. The number of operations is uniformly sampled from 1-10. The starting value is uniformly sampled from 0-20. All numeric values are restricted inclusively to 0-20. The operations are uniformly sampled from $\{+, -\}$ when the cumu val is in the range 1-19. When 0 and 20 the operations are "+" and "-" respectively. The operands are uniformly sampled from the set that restricts the next cumu val to the range 0-20. The cumu val is shown after the "=" for each operation. The "," token follows the cumu val until the end of the sequence in which the E token replaces the comma. The model must predict the "=" tokens, cumu vals, commas, and the E token for a trial to be correct. We use a base 21 token system so that all values correspond to a single token.

Arithmetic Results We include a MAS analysis between Arithmetic GRUs and GRUs trained on the Numeric Equivalence tasks (see Figure 6). The leftmost panel shows that we can successfully align the Cumu Val, and the Rem Ops variables between and within the Arithmetic GRUs. The middle panel shows that MAS can successfully align the Count with the Rem Ops variables between GRUs trained on the Multi-Object and Arithmetic tasks respectively. These results are qualified by the lower IIA alignment between the Count and the Cumu Val variables. We see that when we perform MAS only on Cumu Val values that are shared with possible the Rem Ops values (Low CumuVal), the results are much higher but still do not match the results from Rem Ops. These findings are consistent with the hypothesis that these GRUs are using different types of numeric representations for arithmetic than incremental counting.

A.7 Symbolic Variables

Inspired by DAS, MAS has the ability to find alignments for specific types of information by conditioning the counterfactual sequences specific causal variables (i.e. the count of the sequence in the numeric equivalence tasks).

In all numeric equivalence tasks, we prevent interventions on representations resulting from the BOS, T, and EOS tokens. In the arithmetic task, we only perform interventions on representations after the "," token. We perform MAS using each of the following causal variables, where the corresponding task is denoted in parentheses:

1. **Full** (Arithmetic/Num Equivalence/Modulo/Rounding): Refers to cases in which we transfer all causally relevant information between models (not all activations).

2. **Count** (Num Equivalence/Modulo/Rounding): The difference between the number of observed demo tokens and the number of response tokens in the sequence. Example: the following sequences have a Count of 2 at the last token: "B D D" ; "B D D D T R"
3. **Count** (Modulo): The number of observed demo tokens when in the demo phase, and modulo 4 of the number of demo tokens minus the number of response tokens when in the response phase. Example: the following sequences have a Count of 2 at the last token: "B D D" ; "B D D D D D T R"
4. **Count** (Rounding): The number of observed demo tokens when in the demo phase, and the number of demo tokens rounded to the nearest multiple of 3 minus the number of response tokens when in the response phase. Example: the following sequences have a Count of 2 at the last token: "B D D" ; "B D D D D D T R"
5. **Cumu Val** (Arithmetic): The cumulative value of the arithmetic sequence in the Arithmetic task. Example: if we substitute in a value of 3 at the "," token in the sequence "B 2 Op 3 + 5 = 8 ,," the counterfactual sequence could be "B 2 Op 3 + 5 = 8 , + 2 = 5 E".
6. **Rem Ops** (Arithmetic): The remaining number of operations in the arithmetic sequence. Example: we substitute in a value of 1 at the "," token in the sequence "B 3 Op 3 + 5 = 8 ,," the counterfactual sequence could be "B 3 Op 3 + 5 = 8 , + 1 = 9 E".

A.8 Gram-Schmidt Intervention Proof

We set out to prove the following:

$$\mathcal{R}_i^{-1}((1 - D_i)\mathcal{R}_i h_{trg,t}^{(i)} + D_j \mathcal{R}_j h_{src,u}^{(j)}) = h_{trg,t}^{(i)} + Q_i(-Q_i^\top h_{trg,t}^{(i)} + Q_j^\top h_{src,u}^{(j)}) \quad (20)$$

Where i and j indicate the model indices, src and trg indicate which is the source of information and which is the receiver of information, t and u are integers referring to the step in the target and source sequences from which the tokens were obtained, $\mathcal{R}_i \in R^{d \times d}$ is an orthonormal matrix, $D_i \in R^{d \times d}$ is a diagonal binary matrix with d_{var} nonzero elements, each $h \in R^d$ is a latent state vector, and $Q \in R^{d \times d_{var}}$ is a matrix composed of d_{var} orthogonal column vectors of unit length. We also assume that $\begin{bmatrix} Q_k^\top \\ 0 \end{bmatrix} = D_k \mathcal{R}_k$ where $D_k = \begin{bmatrix} I & 0 \\ 0 & 0 \end{bmatrix}$ and $I \in R^{d_{var} \times d_{var}}$ is an identity matrix. The intervened vector $v_{trg,t}^{(i)}$ for a given intervention is calculated as follows:

$$v_{trg,t}^{(i)} = \mathcal{R}_i^{-1}((1 - D_i)\mathcal{R}_i h_{trg,t}^{(i)} + D_j \mathcal{R}_j h_{src,u}^{(j)}) \quad (21)$$

$$v_{trg,t}^{(i)} = \mathcal{R}_i^\top (1 - D_i)\mathcal{R}_i h_{trg,t}^{(i)} + \mathcal{R}_i^\top D_j \mathcal{R}_j h_{src,u}^{(j)} \quad (22)$$

$$v_{trg,t}^{(i)} = \mathcal{R}_i^\top \mathcal{R}_i h_{trg,t}^{(i)} - \mathcal{R}_i^\top D_i \mathcal{R}_i h_{trg,t}^{(i)} + \mathcal{R}_i^\top D_j \mathcal{R}_j h_{src,u}^{(j)} \quad (23)$$

$$v_{trg,t}^{(i)} = h_{trg,t}^{(i)} + \mathcal{R}_i^\top (-D_i \mathcal{R}_i h_{trg,t}^{(i)} + D_j \mathcal{R}_j h_{src,u}^{(j)}) \quad (24)$$

$$v_{trg,t}^{(i)} = h_{trg,t}^{(i)} + \mathcal{R}_i^\top \left(\begin{bmatrix} Q_i^\top \\ 0 \end{bmatrix} h_{trg,t}^{(i)} + \begin{bmatrix} Q_j^\top \\ 0 \end{bmatrix} h_{src,u}^{(j)} \right) \quad (25)$$

$$v_{trg,t}^{(i)} = h_{trg,t}^{(i)} + \mathcal{R}_i^\top \left(\begin{bmatrix} I \\ 0 \end{bmatrix} Q_i^\top h_{trg,t}^{(i)} + \begin{bmatrix} I \\ 0 \end{bmatrix} Q_j^\top h_{src,u}^{(j)} \right) \quad (26)$$

$$v_{trg,t}^{(i)} = h_{trg,t}^{(i)} + \mathcal{R}_i^\top \left[\begin{bmatrix} I \\ 0 \end{bmatrix} (-Q_i^\top h_{trg,t}^{(i)} + Q_j^\top h_{src,u}^{(j)}) \right] \quad (27)$$

(28)

Here we note that if we set $S_k = [I \ 0]$ then $Q_k^\top = S_k \mathcal{R}_k$. Thus, we can now write the following:

$$v_{trg,t}^{(i)} = h_{trg,t}^{(i)} + \mathcal{R}_i^\top \left[\begin{bmatrix} I \\ 0 \end{bmatrix} (-Q_i^\top h_{trg,t}^{(i)} + Q_j^\top h_{src,u}^{(j)}) \right] \quad (29)$$

$$v_{trg,t}^{(i)} = h_{trg,t}^{(i)} + \mathcal{R}_i^\top S_i^\top (-Q_i^\top h_{trg,t}^{(i)} + Q_j^\top h_{src,u}^{(j)}) \quad (30)$$

$$v_{trg,t}^{(i)} = h_{trg,t}^{(i)} + Q_i(-Q_i^\top h_{trg,t}^{(i)} + Q_j^\top h_{src,u}^{(j)}) \quad (31)$$

And our proof is finished.